



Structure, indentation and corrosion characterizations of high-silicon Ni–Si nano-composite coatings prepared by modified electrodeposition process

Morteza ALIZADEH, Alireza TEYMURI

Department of Materials Science and Engineering,
Shiraz University of Technology, Modarres Blvd., 71557-13876, Shiraz, Iran

Received 4 April 2018; accepted 18 December 2018

Abstract: Ni–Si nano-composite coatings with various silicon contents were prepared by a modified electrodeposition process using electrolytes containing ball-milled Si/Ni particles. The effects of the concentration of the ball-milled Si/Ni particles in the electrolyte on the silicon content, structure, microhardness and corrosion behaviors of the coatings were investigated. Scanning electron microscopy and X-ray diffractometry were used for structural characterization. Also, the microhardness and corrosion behaviors of the deposited coatings were evaluated. According to the results, the Si level reaches about 10 wt.% in the coating, which is a significant content of Si incorporation for electrodeposition. It was also found that the crystallite size of the coatings was progressively decreased and the hardness was increased, by increasing the content of Si. Typically, the crystallite size and microhardness of the Ni–10wt.%Si coating were 0.39 and 2.1 times those of the pure Ni coating, respectively. Also, the results showed that there is an optimal content of Si to meet the best acidic corrosion resistance of the coatings.

Key words: Ni–Si composite coating; electrodeposition; structure; corrosion behavior; microhardness

1 Introduction

Metal-matrix composite coatings are deposited on metallic substrates in order to improve various function properties, such as hardness, oxidation resistance, wear resistance, and self-lubricating [1]. Composite coatings are deposited by various surface engineering techniques. In recent years, several methods like thermal spraying, laser cladding, physical vapor deposition (PVD) and electrodeposition have been employed to produce pure metal and metal-matrix composite coatings [2–4]. Among these methods, electrodeposition has some advantages, such as environmental friendliness, low cost, high throughput, energy-save, and purification control [3]. Therefore, this technique is widely used in the production of alloys and composite coatings [5–7]. The properties of the coatings produced by the electrodeposition method depend on parameters such as bath concentration, current density, pH, temperature, and type and concentration of second phase particles in the suspension [1,5–8]. It has been reported that by increasing the content of second phase particles in the electrolyte bath, the fraction of the particles in the

deposited coating is initially increased and then reduced [9]. The reduction in the deposited particles has been attributed to an increase in the particles agglomeration and elastic collisions among the particles [9].

Various particles such as oxides (TiO_2 , Al_2O_3 , CeO_2 and ZrO_2), carbides (SiC, TiC and WC), nitrides, and metallic powders (Si, W, Co and Mo) have been added to metal matrix composite coatings [2–12]. Each second phase particle forgives a specific character to the produced composites. Some particles improve the mechanical properties (such as hardness and wear resistance) of the coatings [7]. Some others enhance the corrosion resistance of the coatings [10], and some of them improve several properties simultaneously [6,7,9]. For instance, silicon particles can improve the microhardness and oxidation resistance of the coating [13]. YU et al [14] have deposited a Ni–Si coating on $\text{Ti}_6\text{Al}_4\text{V}$ alloy and observed that this coating increased the oxidation and corrosion resistances of $\text{Ti}_6\text{Al}_4\text{V}$ alloy. GRUNLING and BAUER [15] have shown that the presence of Si in a Ni matrix can decrease the oxidation rate of the Ni matrix due to limited ionic transport. Therefore, Ni–Si coatings can protect

substrates from oxidation. The aim of this research is the codeposition of silicon particles with various contents onto a nickel matrix. In this regard, ball-milled Si/Ni particles with various concentrations were used as the reinforcement in the electrolyte for the preparation of Ni–Si nanocomposite coatings. Afterwards, the effects of the Si/Ni particle concentration in the suspension on the silicon content, structure, microhardness, and corrosion behavior of the produced composite coatings were investigated.

2 Experimental

2.1 Powder preparation

In this study, silicon (Merck, >99.5 wt.%) and nickel (Merck, >99.5 wt.%) powders were mixed at mass ratio of 80:20 and then milled in a planetary ball mill (Diba 75D) with steel vial (95 mL) and balls (6 balls of 20 mm and 12 balls of 10 mm in diameter) under an argon atmosphere. The milling speed was selected to be 450 r/min and the ball-to-powder mass ratio of about 20:1 was used. It is noticeable that in order to reduce the amount of contamination, the powders obtained from the third milling duration were used for the electrodeposition process.

2.2 Electrodeposition

A Watts Ni bath containing the Si/Ni particles was used for the deposition of coatings on low carbon steel specimens. The composition of the bath is listed in Table 1. Also, electrodeposition parameters are summarized in Table 2. The solution was prepared from analytic grade chemicals and double distilled water.

Table 1 Composition of bath solution

Component	Concentration/(g·L ⁻¹)
NiSO ₄ ·6H ₂ O	320
NiCl ₂ ·6H ₂ O	40
H ₃ BO ₃	50
C ₁₂ H ₂₅ SO ₄ NaS (SDS)	0.1
Si/Ni particles	0–50

Table 2 Experimental electrodeposition parameters

Parameter	Value
Current density/(A·dm ⁻²)	2
pH	4±0.2
Temperature/°C	50±1
Stirring speed/(r·min ⁻¹)	250
Deposition time/min	60

The Si/Ni particles were added to the prepared Watts bath, while the bath was stirred at 500 r/min for 18 h before the deposition process. During the composite

deposition process, stirring did not stop while its speed was 250 r/min. The volume of the electrolyte was 750 mL. The anode in this work was a pure nickel plate of 50 mm × 30 mm × 4 mm in size and the cathode was low carbon steel plate of 20 mm × 15 mm × 1.5 mm in size. The surface ratio of the anode to the cathode was selected to be about 5:1 and the distance of about 3 cm between them was used. Before the deposition process, surface preparation processes, i.e. mechanical polishing, cleaning by acetone, and activating by hydrochloric acid, were done on the cathode surface.

2.3 Characterization

To investigate the particle size and distribution of the milled Si/Ni powders, a dynamic light scattering particle size analyzer (Horiba model) was used. It is noticeable that the measurement of the size distribution was carried out after settling of micron-sized particles. Therefore, the reported size distribution was for nano-size particles.

The microstructure of the coatings was assessed by using a VEGA3.TESCAN scanning electron microscope (SEM). For the investigation of the coating composition, an energy dispersive X-ray spectroscopy (EDS) was used. The EDS examinations were done in three distinct points of the coatings.

The structural investigations of the deposited coatings were carried out by an X-ray diffraction instrument (XRD, Bruker Advance 2 with the Cu K_{α1} radiation, 40 kV and 40 mA). The step time and step size were selected to be 3 s and 0.05°, respectively. To study the effect of the Si particles on the texture of the Ni matrix, the texture coefficient (*TC*) was estimated by the following equation [16]:

$$TC(hkl) = \frac{R_1(hkl)}{R_2(hkl)} \quad (1)$$

where R_1 and R_2 were calculated by Eqs. (2) and (3), respectively [16]:

$$R_1(hkl) = \frac{I(hkl)}{\sum_{i=1}^n I(h_i k_i l_i)} \times 100\% \quad (2)$$

$$R_2(hkl) = \frac{I_s(hkl)}{\sum_{i=1}^n I_s(h_i k_i l_i)} \times 100\% \quad (3)$$

where $I(hkl)$ is the intensities of the (*hkl*) planes diffracted in the XRD pattern of the nickel coating specimen, $I_s(hkl)$ is the intensities of the (*hkl*) planes diffracted in the XRD pattern of the standard nickel specimen, and n is the number of reflections used in the calculation. In the present study, (111), (200) and (220) planes were considered for the texture coefficient

calculation ($n=3$). The relative texture coefficient (RTC) was also estimated by the following equation [16]:

$$RTC(hkl) = \frac{TC(hkl)}{\sum_{i=1}^n TC(h_i k_i l_i)} \times 100\% \quad (4)$$

The Scherrer equation [17] was also used to determine the crystallite size of the coatings. The corrosion properties of the prepared coatings were investigated by an Ivium potentiostat/galvanostat device. During the corrosion experiments, the coated samples, a platinum plate, and a Ag/AgCl electrode were used as the working, auxiliary, and reference electrodes, respectively. The corrosion tests were done in a 0.5 mol/L Na_2SO_4 solution at 25 °C. The polarization curves were plotted by the Ivium software and the corrosion properties of corrosion potential and current density were estimated from the polarization curves.

The Vickers microhardness of the prepared coatings was measured under a load of 50 g and a holding time of 10 s. Six measurements were carried out for each coating and average of the results was reported.

3 Results and discussion

3.1 Effect of Si/Ni particle concentration in bath on Si content in coatings

Figure 1 shows the SEM images of the Si/Ni powder mixture milled for 21 h at two magnifications. As it can be seen from Fig. 1(b), the milled powders have an equiaxed morphology and their size is in a wide range (Fig. 1(a)). Figure 2 shows the size distribution of the milled powders after settling of micron-size particles, confirming that there are nano-sized powders in the milled powder mixture.

Figure 3 shows the influence of the Si/Ni concentration in the electrolyte on the silicon content of the prepared Ni–Si composite coating. With increasing the Si/Ni concentration in the electrolyte to 40 g/L, the amount of the silicon particles adsorbed on the growing deposit surface is increased, whereas the silicon content is decreased after that concentration. As it can be seen, the silicon particle content is increased from 0 to about 9 wt.% when the Si/Ni concentration in the bath is increased from 0 to 40 g/L. During the electrodeposition process, ionic clouds are adsorbed on the Si/Ni particles surface, encouraging the Si/Ni particles to move towards the cathode. The particles passing from the electrical double-layer, are adsorbed on the deposited nickel matrix and then are entrapped by the growing nickel matrix [18]. It is obvious that the increase of the particle concentration in the bath enhances the adsorption chance of the particles to the growing coating matrix. However, when the Si/Ni concentration in the plating solution

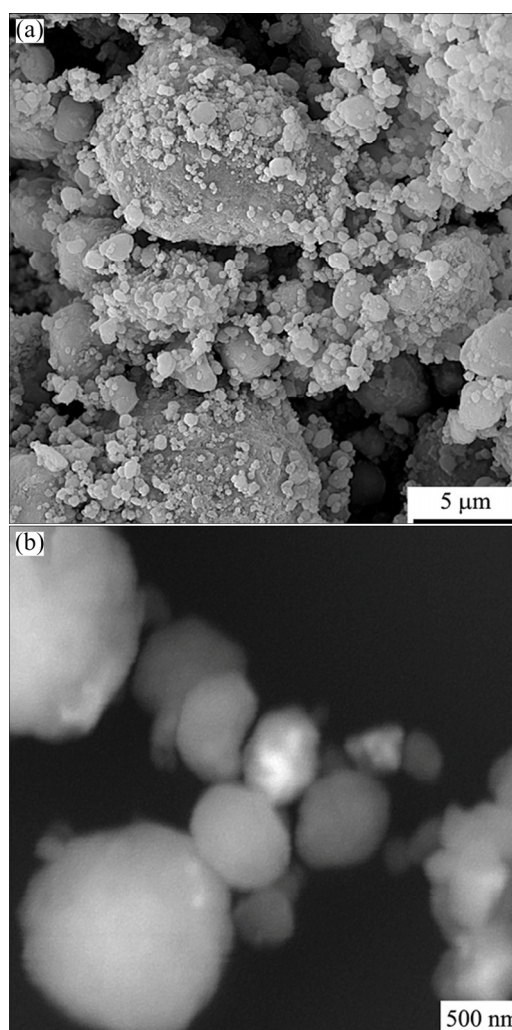


Fig. 1 SEM images of Si/Ni powder milled for 21 h: (a) Lower magnification; (b) Higher magnification

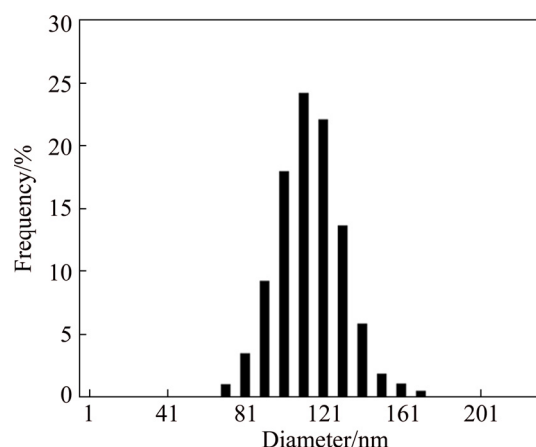


Fig. 2 Particle size distribution of Si/Ni powder milled for 21 h

exceeds 50 g/L, the Si content in the deposit is decreased. This behavior is attributed to the particles agglomeration in the electrolyte and the increase in the viscosity of the bath when the concentration of the Ni/Si particles is increased [9,19,20].

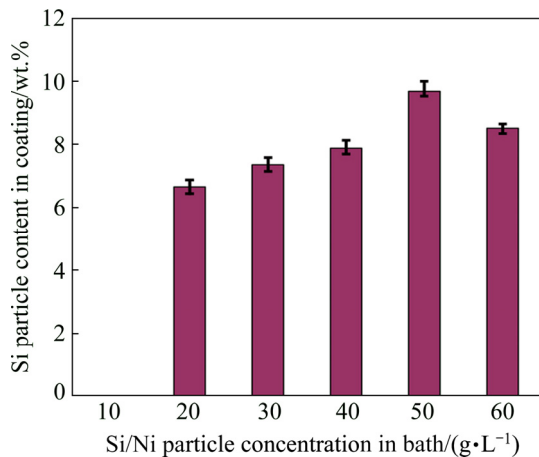


Fig. 3 Si particle content in prepared coating as function of Si/Ni powder concentration in electrolyte

3.2 XRD patterns

Figure 4 shows the XRD patterns of the coatings prepared at 0, 10, 20 and 40 g/L of the Si/Ni reinforcement in the bath. The peaks of nickel and silicon have appeared in the patterns (Fig. 4(b)). This shows that the silicon particles are successfully incorporated in the nickel matrix during the electrodeposition process. It should be noted that the intensity of the silicon peaks is increased with increasing the Si/Ni concentration in the bath. This indicates the presence of higher silicon percentages in the coatings. From Fig. 4, it is apparent that the (200) plane has the maximum intensity. The incorporated silicon particles decrease the intensity of the (200) plane, whereas they increase the intensity of the (111) plane. In fact, the silicon particles as the second phase change the texture of the nickel matrix from the soft-mode to a preferred orientation [21].

The texture coefficient (TC) and relative texture coefficient (RTC), calculated using Eqs. (1) and (4), are summarized in Table 3. From Table 3, it can be seen that the TC of the (200) plane in the pure Ni is greater than 1, meaning a preferred orientation [16]. It is obvious that when the silicon particles are embedded in the Ni matrix, the TC of the (200) plane becomes less than 1. This shows that the (200) plane in the composite samples has no preferred orientation, whereas the (111) plane shows a preferred orientation when the silicon particles are added to the deposit. The RTC results also confirm that the preferred orientation is changed from (200) to (111) planes when the silicon particles are added to the coating.

An important effect of the silicon particles on the deposited coatings is the decrease of the matrix crystallite size. As it can be seen from the diffraction patterns (Fig. 4), peak broadening occurs when the silicon particles are incorporated in the nickel matrix. It is obvious that by increasing the silicon particles in the

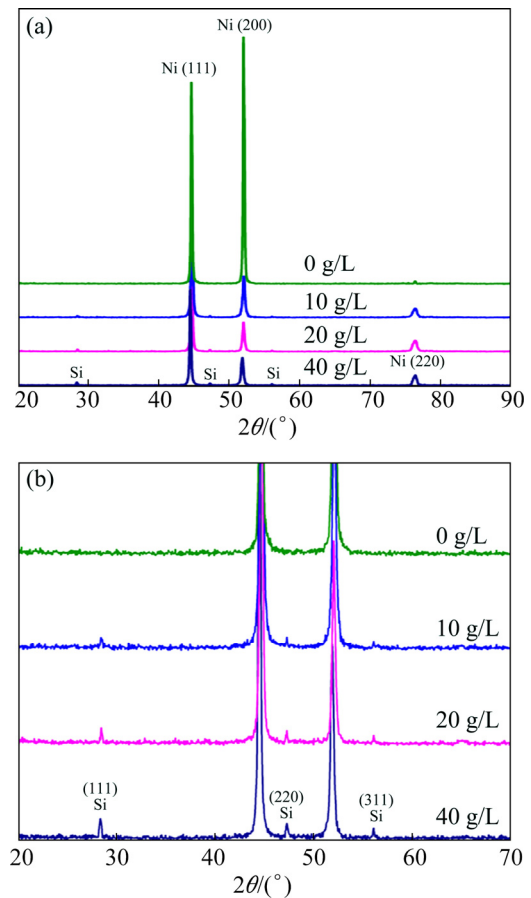


Fig. 4 XRD patterns of coatings prepared at different reinforcement concentrations (a) and prepared coating clearly showing silicon peaks (b)

Table 3 Effect of Si/Ni powder concentration on texture coefficient (TC) and relative texture coefficient (RTC) of deposited coatings

Si/Ni concentration in bath/(g·L ⁻¹)	TC (hkl)			RTC (hkl)/%		
	(111)	(200)	(220)	(111)	(200)	(220)
0	0.729	2.115	0.058	25.1	72.9	2.0
10	1.224	0.783	0.365	51.6	32.9	15.5
20	1.207	0.695	0.623	47.8	27.5	24.7
40	1.152	0.797	0.682	43.8	30.3	25.9

prepared coating, the peak broadening is increased. This shows that the embedded silicon particles decrease the crystallite size of the coating [22]. The variation of the crystallite size versus the Si/Ni concentration in the bath is illustrated in Fig. 5. According to Fig. 5, by adding the silicon particles to the bath from 0 to 40 g/L, the coating crystallite size is decreased from 176 to 75 nm. It has been reported that the crystallite size of the coatings during the electrodeposition process is determined by a competition between crystal nucleation and growth [7]. It is evident that when the nucleation rate is increased,

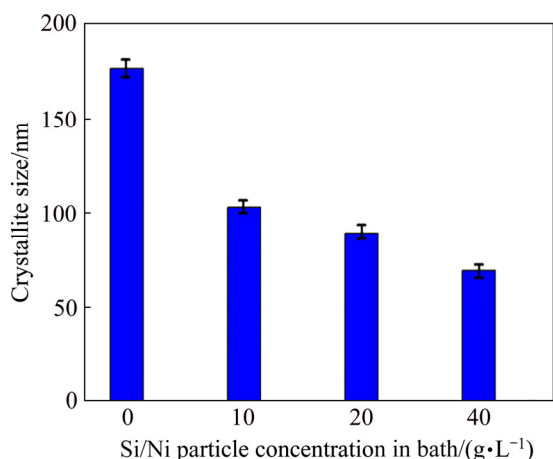


Fig. 5 Crystallite size of coating vs concentration of Si/Ni powder in deposition bath

the growth rate and consequently the crystallite size are decreased. Since silicon particles as the second phase increase the nucleation rate of nickel crystals, they inhibit the nickel crystals growth [7]. As a result, the nickel crystallite size of the reinforced coatings is smaller than that of the pure nickel coating. Also, the

coating reinforced with the maximum particle content (40 g/L Ni/Si) has the minimum crystallite size.

3.3 Surface and cross-sectional morphologies of coatings

The surface morphologies of the deposited coatings obtained from the bath with various Si/Ni particle concentrations are shown in Fig. 6. It can be seen from Fig. 6 that by the incorporation of the silicon particles into the nickel coating, the surface morphology is changed from a uniform polyhedral feature (Fig. 6(a)) to a non-uniform protruding one. In fact, the presence of the Si/Ni particles embedded in the nickel matrix changes the growth regime of polynomial observed for the pure nickel coating to epitaxial for the composite coating [23–25]. However, it is evident that by increasing the silicon content, the surface heterogeneity of the coatings is increased (see Figs. 6(b–d)). Moreover, when the particle concentration in the bath is increased, the number of agglomerated particles in the coatings is increased, causing a more heterogeneity of the coating [26].

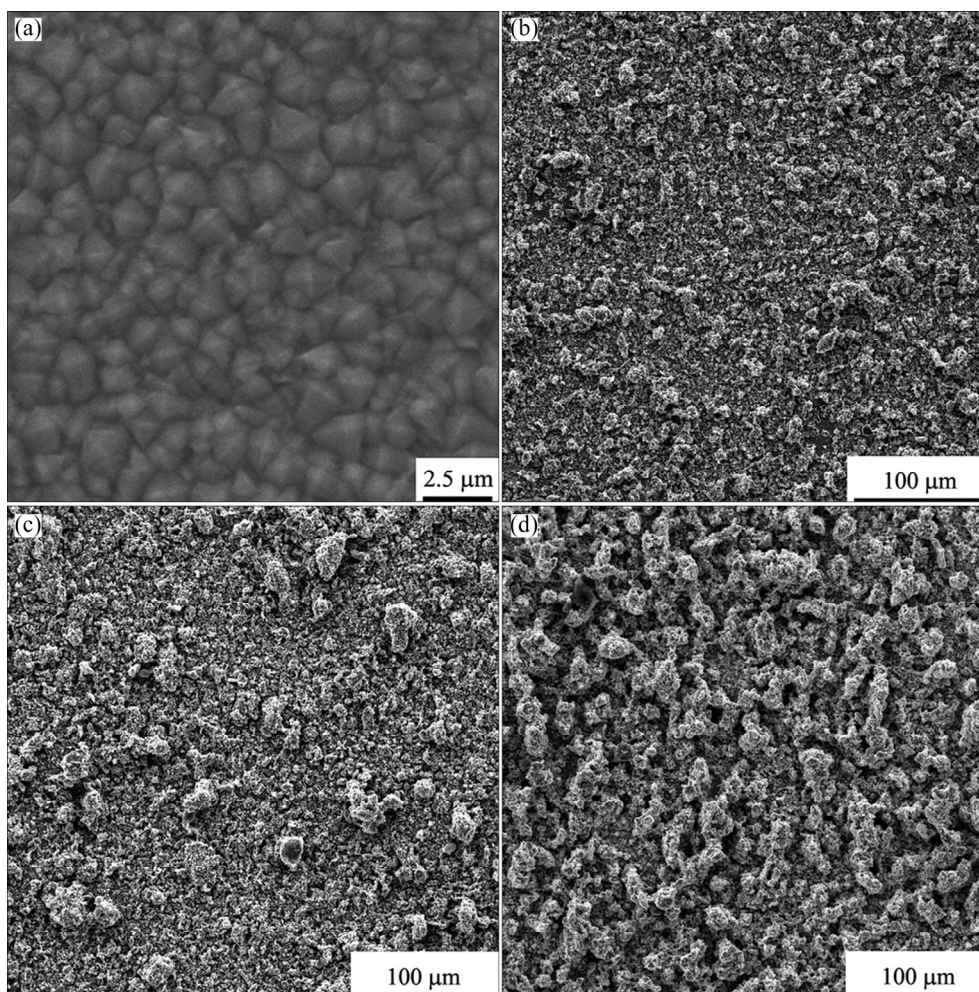


Fig. 6 SEM surface microstructures of pure nickel and composite coatings with average thickness of 30 μm and different Si/Ni concentrations in deposition bath: (a) Pure nickel; (b) 10 g/L; (c) 20 g/L; (d) 40 g/L

The cross-sectional SEM morphologies of the prepared Ni–Si composite coatings are shown in Fig. 7. It can be seen from Fig. 7 that the average thickness of the coating is about 30 μm . It is apparent that the coatings show a compact structure and no defects (cracks or voids) are observed at the interface of the coating/substrate. This means that a good adhesion between the coating and substrate has been created. The cross-sectional images of the prepared coatings also confirm the incorporation of the Si particles into the nickel matrix during the electrodeposition process (see Fig. 7(d)). The SEM images and elemental distribution EDS maps of the Ni–Si composite coatings obtained at 10, 20 and 40 g/L of the Si/Ni reinforcement in the bath are shown in Fig. 8. It can be seen from Figs. 7 and 8 that a uniform distribution of the silicon particles has been achieved in the deposited Si–Ni composite coatings. Figures 7 and 8 also confirm that by increasing the Si/Ni particles concentration in the bath, the silicon content in the coatings is increased. This result is consistent with the XRD results (see Fig. 4). In fact, by increasing the Si/Ni particles concentration in the bath, the number of the Si/Ni particles attached on the cathode surface and thus their content in the deposit are increased. It is noteworthy that the Ni^{2+} ions adsorbed on the Si/Ni particles have a significant role in the attachment of the particles on the cathode surface [23,26].

3.4 Effect of Si/Ni particle concentration on coating micro-hardness

Figure 9 shows the microhardness values of the composite coatings prepared at various Si/Ni particle concentrations in the deposition bath. The microhardness experiments were done on the cross-sections of coatings. It is obvious that the composite coatings have higher microhardness value, compared with the pure nickel coating. Typically, the microhardness value of the 40 g/L composite is about 2.1 times as high as that of the pure nickel (0 g/L) coating. Also, by increasing the particle concentration value in the deposition bath from 10 to 40 g/L, the microhardness value is increased from about HV 260 to HV 372. The improvement in the microhardness of coatings in the presence of the second phase particles can be attributed to the following mechanisms: (1) grain refinement strengthening (the Hall–Petch equation), (2) solid solution strengthening, (3) dispersion strengthening due to the Orowan mechanism, and (4) crystal orientation [9,27].

Since the microhardness of the silicon particles is higher than that of the pure nickel, they can increase the microhardness of coatings. In this mechanism, the incorporated hard silicon particles constrain the deformation of the nickel matrix and consequently increase the strength and hardness of the matrix [28]. In this case, both the matrix and hard silicon particles carry

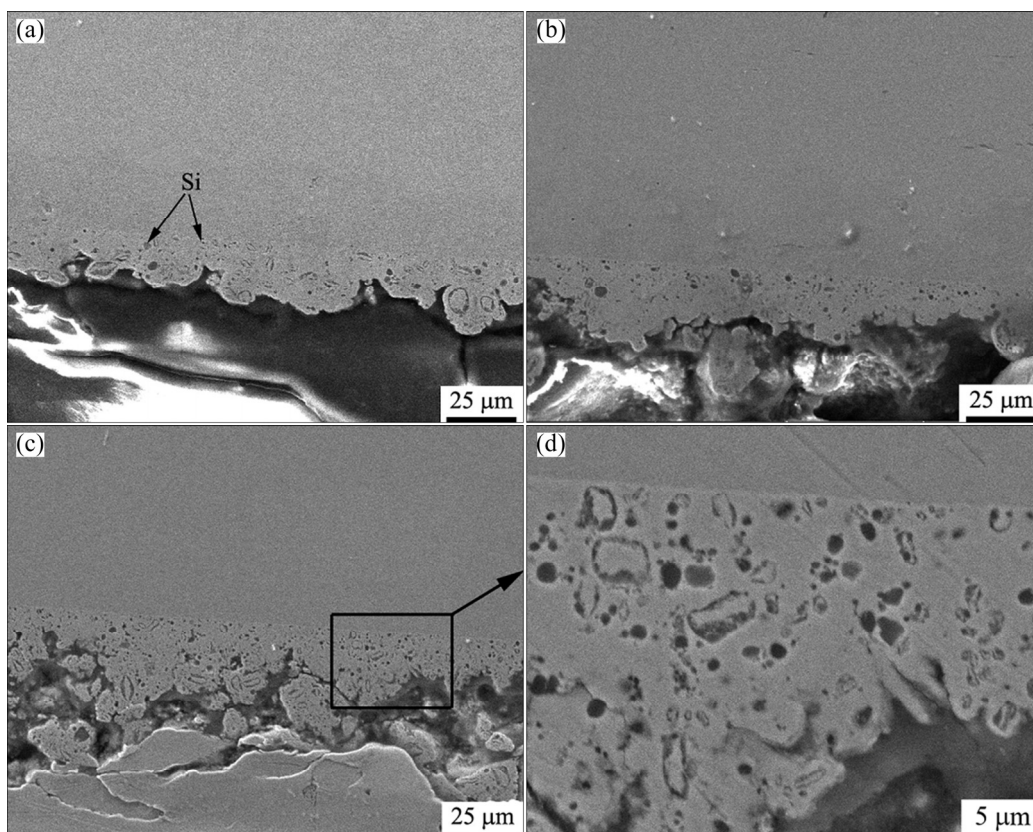


Fig. 7 Cross-sectional SEM morphologies of composite coatings prepared at different Si/Ni concentrations in bath: (a) 10 g/L; (b) 20 g/L; (c, d) 40 g/L

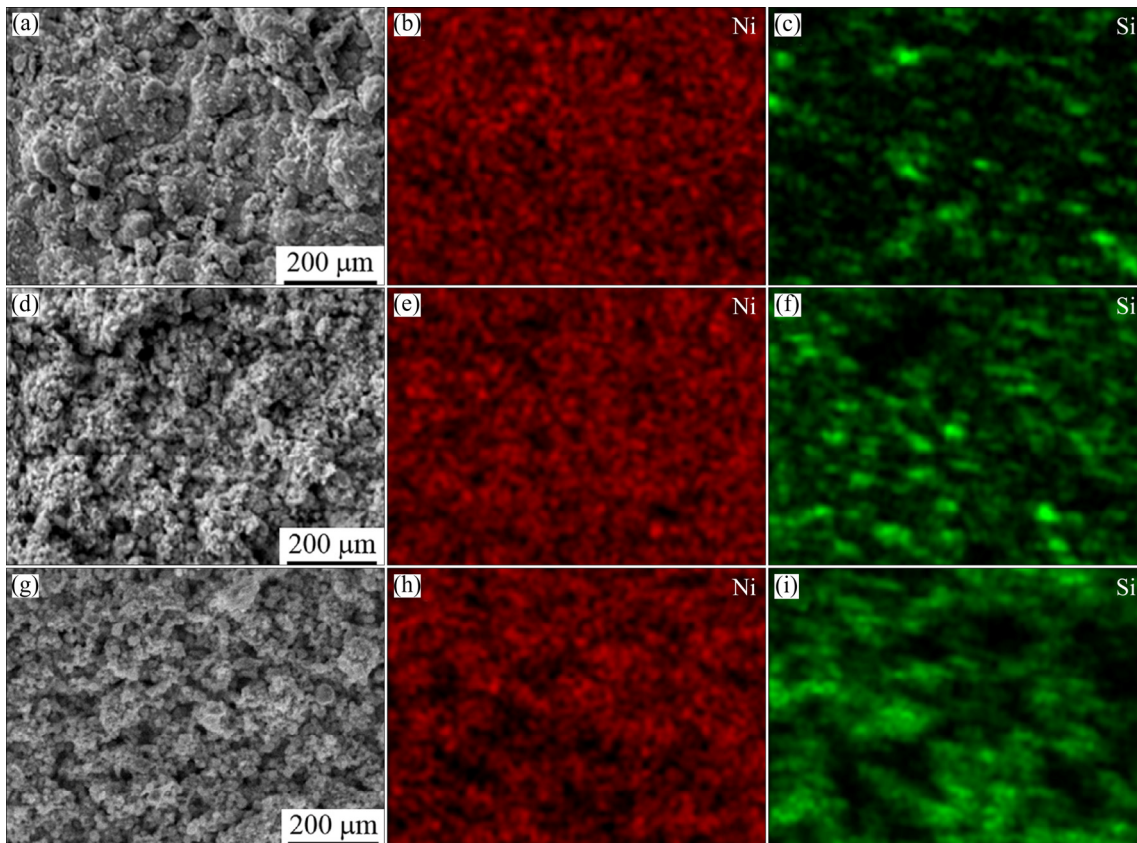


Fig. 8 SEM micrographs (a, d, g) and EDS maps (b, c, e, f, h, i) of Ni–Si composite coatings deposited at different Si/Ni particle concentrations: (a, d, g) 10 g/L; (b, e, f) 20 g/L; (c, f, i) 40 g/L

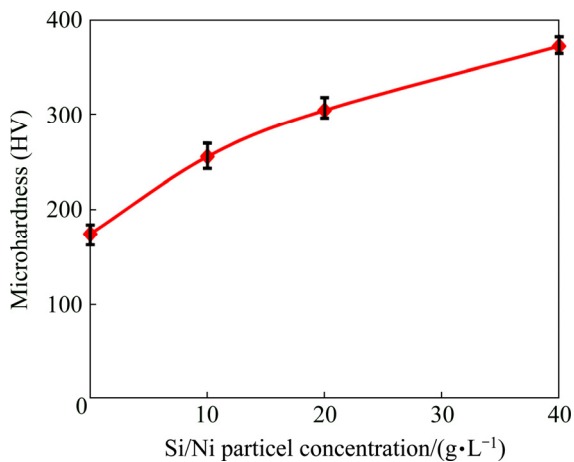


Fig. 9 Microhardness values of prepared coatings vs Si/Ni particle concentration in deposition bath

applied loads. In addition, according to the XRD results, by the incorporation of the Si particles into the nickel matrix, the nickel crystallite size is decreased. Therefore, the microhardness of the produced coatings is increased, based on the Hall–Petch equation [6]:

$$HV = H_0 + kd^{-1} \quad (5)$$

where HV is the hardness, d is the average nickel crystallite size, and H_0 and k are constants. In the

Hall–Petch mechanism, the grain boundaries have an important role in strengthening. When the crystallite size is decreased, the grain boundaries are increased. The grain boundaries behave as barriers against the dislocations motion; therefore, the coating hardness is increased.

In the present work, the microhardness of the coatings may be also increased by the Orowan mechanism. In this mechanism, the nanoparticles resist against the dislocation movement and increase the microhardness of the coatings [29]. It can be seen from Figs. 1 and 2 that the ball-milled powders consist of nano- and micron-sized Si/Ni particles. Therefore, the presences of the nano-sized particles in the deposited coatings can active the Orowan strengthening mechanism and increase the coatings microhardness. However, since the majority of the Si/Ni particles are micron-sized, the role of the Orowan mechanism in the increase of microhardness is not significant [29].

3.5 Corrosion properties

The corrosion behavior of the deposited pure nickel and composite coatings was investigated in an acidic solution (0.5 mol/L Na_2SO_4) with a pH value of about 2. The polarization curves of the tested samples are shown

in Fig. 10. Also, the corrosion parameters including corrosion potential and corrosion current density, estimated from the polarization curves, are listed in Table 4. It is seen that the corrosion potential of the 5 and 10 g/L composite coatings is close to that of the pure nickel coating. However, by increasing the Si/Ni particle concentration in the bath up to 40 g/L, the corrosion potential of the coatings is decreased due to the increase in the fraction of micro-pores on the coatings surface (see Fig. 6).

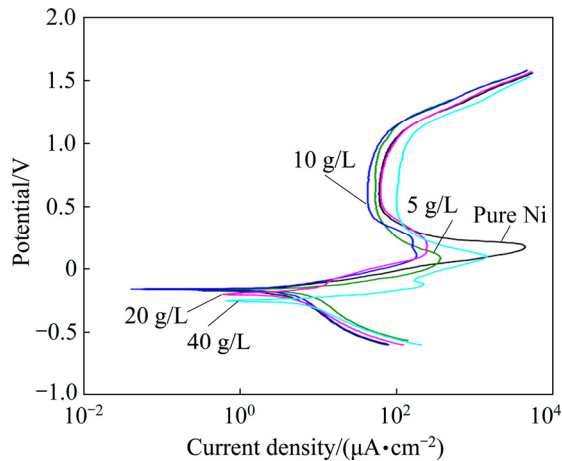


Fig. 10 Potentiodynamic polarization curves of prepared coatings in 0.5 mol/L Na_2SO_4 solution

Table 4 Corrosion parameters derived from potentiodynamic polarization data

Particle concentration in bath/(g·L ⁻¹)	$\phi_{\text{corr}}/\text{V}$	$J_{\text{corr}}/(\mu\text{A}\cdot\text{cm}^{-2})$
0	-0.17	5.0
5	-0.16	3.5
10	-0.15	3.0
20	-0.20	4.5
40	-0.25	6.0

The variation in the corrosion current density of the deposited coatings is shown in Table 4. It is obvious that the corrosion current density of the coatings is firstly decreased by increasing the Si/Ni particle concentration in the bath (up to 10 g/L). Indeed, the incorporation of the Si/Ni particles into the nickel matrix improves the corrosion resistance of the pure nickel. The improvement of the corrosion resistance is attributed to the modification of the coating structure by the reinforcement particles [22]. Being consistent with Fig. 5, the grain refinement occurs by the incorporation of the Si/Ni into the matrix and the grain boundaries are increased. It has been reported that when grain refinement occurs, the corrosive solution should pass a longer path to reach the substrate. Therefore, the corrosion resistance is increased [22].

Concerning Table 4, the corrosion current density is increased again by increasing the particle concentration from 10 g/L. The increase in the fraction of the particles in the coatings leads to the increase of micro-pores on the surface of the coatings. The presence of these defects on the surface of the coatings causes to the more exposure of the steel substrate to the corrosion medium. In this case, a galvanic coupling is created between the substrate and coating, and thereby the corrosion resistance is decreased.

4 Conclusions

(1) The amount of the incorporated Si particles depended on the Si/Ni powder concentration in the bath. The Si content in the composite coatings was enhanced when the concentration of the particles in the electrolyte increased up to 40 g/L.

(2) The surface non-homogeneity was increased when the content of the silicon particles was raised. The Si particles were homogeneously embedded in the nickel matrix and changed the texture of the coatings.

(3) The coating crystallite size was a function of the Ni/Si particles concentration in the bath, and decreased when the particle concentration was increased.

(4) The presence of the Ni/Si particles into the nickel matrix affected positively the microhardness and raised it to HV 372 when the Si content was about 10 wt.%. The corrosion resistance of the coatings was a function of the incorporated Ni/Si particles concentration.

References

- [1] ZHANG Z, WU X, JIANG C, MA N. Electrodeposition of Ni matrix composite coatings containing ZrC particles [J]. *Surface Engineering*, 2014, 30: 21–25.
- [2] KIM S K, OH T S. Electrodeposition behavior and characteristics of Ni-carbon nanotube composite coatings [J]. *Transactions of Nonferrous Metals Society of China*, 2011, 21: 68–72.
- [3] ZHOU Y U, ZHANG S, NIE L L, ZHU Z J, ZHANG J Q, CAO F H, ZHANG J X. Electrodeposition and corrosion resistance of Ni-P-TiN composite coating on AZ91D magnesium alloy [J]. *Transactions of Nonferrous Metals Society of China*, 2016, 26: 2976–2987.
- [4] ZAMANI M, AMADEH A, LARI BAGHAL S M. Effect of Co content on electrodeposition mechanism and mechanical properties of electrodeposited Ni-Co alloy [J]. *Transactions of Nonferrous Metals Society of China*, 2016, 26: 484–491.
- [5] KIM S K, YOO H J. Formation of bilayer Ni-SiC composite coatings by electrodeposition [J]. *Surface and Coatings Technology*, 1998, 108: 564–569.
- [6] GRILL C D, KOLLENDER J P, HAS A W. Electrodeposition of cobalt-nickel material libraries [J]. *Physica Status Solidi*, 2015, 212: 1216–1222.
- [7] THIEMIG D, BUND A. Characterization of electrodeposited Ni-TiO₂ nanocomposite coatings [J]. *Surface and Coatings Technology*, 2008, 202: 2976–2984.

- [8] CASCIANO P N S, BENEVIDES R L, SANTANA R A C, CORREIA A N, LIMA-NETO P. Factorial design in the electrodeposition of Co–Mo coatings and their evaluations for hydrogen evolution reaction [J]. *Journal of Alloys and Compounds*, 2017, 723: 164–171.
- [9] LEE H K, LEE H Y, JEON J M. Codeposition of micro- and nano-sized SiC particles in the nickel matrix composite coatings obtained by electroplating [J]. *Surface and Coatings Technology*, 2007, 201: 4711–4717.
- [10] ELKHOSHKHANY N, HAFNWAY A, KHALED A. Electrodeposition and corrosion behavior of nano-structured Ni–WC and Ni–Co–WC composite coating [J]. *Journal of Alloys and Compounds*, 2017, 695: 1505–1514.
- [11] BOSTANI B, PARVINI AHMADI N, YAZDANI S, ARGHAVANIAN R. Co-electrodeposition and properties evaluation of functionally gradient nickel coated ZrO₂ composite coating [J]. *Transactions of Nonferrous Metals Society of China*, 2018, 28: 66–76.
- [12] OLIVEIRA A L M, COSTA J D, SOUSA M B, ALVES J J N, CAMPOS A R N, SANTANA R A C, PRASAD S. Studies on electrodeposition and characterization of the Ni–W–Fe alloys coatings [J]. *Journal of Alloys and Compounds*, 2015, 619: 697–703.
- [13] FELLNER P, CONG P K. Ni–B and Ni–Si composite electrolytic coatings [J]. *Surface and Coatings Technology*, 1996, 82: 317–319.
- [14] YU C, ZHU S, WEI D, WANG F. Oxidation and H₂O/NaCl-induced corrosion behavior of sputtered Ni–Si coatings on Ti₆Al₄V at 600–650 °C [J]. *Surface and Coatings Technology*, 2007, 201: 7530–7537.
- [15] GRUNLING H, BAUER R. The role of silicon in corrosion-resistant high temperature coatings [J]. *Thin Solid Films*, 1982, 95: 3–20.
- [16] BERUBE L P, ESPERANCE G L A. Quantitative method of determining of the degree of texture of zinc electrodeposits [J]. *Journal of the Electrochemical Society*, 1989, 136: 2314–2315.
- [17] AKBAR D. Surface modification of polypropylene (PP) using single and dual high radio frequency capacitive coupled argon plasma discharge [J]. *Applied Surface Science*, 2016, 362: 63–69.
- [18] CELIS J P, ROOS J, BUELENS C. A mathematical model for the electrolytic codeposition of particles with a metallic matrix [J]. *Journal of the Electrochemical Society*, 1987, 134: 1402–1408.
- [19] BAKHIT B, AKBARI A. Synthesis and characterization of Ni–Co/SiC nanocomposite coatings using sediment co-deposition technique [J]. *Journal of Alloys and Compounds*, 2013, 560: 92–104.
- [20] GYFTOU P, PAVLATOU E A, SPYRELLIS N. Effect of pulse electrodeposition parameters on the properties of Ni/nano–SiC composites [J]. *Applied Surface Science*, 2008, 254: 5910–5916.
- [21] SPYRELIS N, PAVLATOU E A, SPANO S, ZOIKIS-KARATHANASIS A. Nickel and nickel–phosphorous matrix composite electrocoatings [J]. *Transactions of Nonferrous Metals Society of China*, 2009, 19: 800–804.
- [22] VAEZI M, SADRNEZHAAD S, NIKZAD L. Electrodeposition of Ni–SiC nano-composite coatings and evaluation of wear and corrosion resistance and electroplating characteristics [J]. *Colloids and Surfaces A*, 2008, 315: 176–182.
- [23] NAPLOSZEK-BILNIK I, BUNIOK A, LAGIEWKA E. Electrolytic production and heat-treatment of Ni-based composite layers containing intermetallic phases [J]. *Journal of Alloys and Compounds*, 2004, 382: 54–60.
- [24] SRIKOMOL S, BOONYONGMANEERAT Y, TECHAPIE-SANCHAROENKIJ R. Electrochemical codeposition and heat treatment of nickel–titanium alloy layers [J]. *Metallurgical and Materials Transactions B*, 2013, 44: 53–62.
- [25] FENG Q, LI T, YUE H, QI K, BAI F, JIN J. Preparation and characterization of nickel nano-Al₂O₃ composite coatings by sediment co-deposition [J]. *Applied Surface Science*, 2008, 254: 2262–2268.
- [26] NAPLOSZEK-BILNIK I, BUDNIOK A, LOSIEWICZ B, PAJAK L, LAGIEWKA E. Electrodeposition of composite Ni-based coatings with the addition of Ti or/and Al particles [J]. *Thin Solid Films*, 2005, 474: 146–153.
- [27] ARUNA S, ANANDAN C, GRIPS V W. Effect of probe sonication and sodium hexametaphosphate on the microhardness and wear behavior of electrodeposited Ni–SiC composite coating [J]. *Applied Surface Science*, 2014, 301: 383–390.
- [28] BENE L, BONORA P L, BORELLO A, MARTELLI S. Wear corrosion properties of nano-structured SiC–nickel composite coatings obtained by electroplating [J]. *Wear*, 2001, 249: 995–1003.
- [29] HAZZLEDINE P. Direct versus indirect dispersion hardening [J]. *Scripta Metallurgica et Materialia*, 1992, 26: 57–58.

改进电沉积法制备高硅 Ni–Si 纳米复合镀层的结构、压痕和腐蚀特性

Morteza ALIZADEH, Alireza TEYMURI

Department of Materials Science and Engineering,
Shiraz University of Technology, Modarres Blvd., 71557-13876, Shiraz, Iran

摘要: 以含有球磨 Si/Ni 颗粒的电解质为原料, 采用改进的电沉积工艺制备不同硅含量的 Ni–Si 纳米复合镀层。研究电解液中球磨 Si/Ni 颗粒浓度对镀层的硅含量、结构、显微硬度和腐蚀行为的影响。采用扫描电镜和 X 射线分析仪对其结构进行表征, 并对镀层的显微硬度和腐蚀行为进行评估。结果表明, 镀层中硅的最高含量可达近 10 wt.%, 这是电沉积中硅的重要掺入量。随着硅含量的增加, 镀层的晶粒尺寸逐渐减小, 硬度增加。其中, Ni–10wt.%Si 镀层的晶粒尺寸和显微硬度分别是纯 Ni 涂层的 0.39 倍和 2.1 倍。结果还表明, 镀层的硅含量存在一个最佳值, 此时其耐酸性腐蚀性能最佳。

关键词: 复合镀层; 电沉积; 结构; 腐蚀行为; 显微硬度

(Edited by Wei-ping CHEN)